催 化 学 报
2011 Chinese Journal of Catalysis Vol. 32 No. 3

文章编号: 0253-9837(2011)03-0418-10 国际版 DOI: 10.1016/S1872-2067(10)60177-5 研究论文: 418~427

介孔-微孔复合材料的水热稳定性及其催化裂化性能

韩 伟, 贾玉心, 熊国兴, 杨维慎

中国科学院大连化学物理研究所催化基础国家重点实验室, 辽宁大连 116023

摘要: 采用无模板剂的溶胶凝胶法制备了一系列具有均一介孔和MFI沸石微孔的复合材料. 与MCM-41相比, 包含silicalite-1沸石结构的复合材料的水热稳定性得到显著改善. 1,3,5-三异丙苯的催化裂化反应结果表明, 与商品HZSM-5沸石相比, 包含ZSM-5沸石结构的复合材料具有更高的催化活性和抗积炭性能. 三异丙苯的转化率和裂化产物的分布主要取决于介孔-微孔复合材料的介孔孔径, 较小的介孔孔径有利于提高转化率和生成更多小分子裂化产物.

关键词: 介孔-微孔复合材料; MFI沸石; 水热稳定性; 1,3,5-三异丙苯; 催化裂化

中图分类号: O643 **文献标识码:** A

Hydrothermal Stability of Meso-microporous Composites and Their Catalytic Cracking Performance

HAN Wei, JIA Yuxin, XIONG Guoxing*, YANG Weishen*

State Key Laboratory of Catalysis, Dalian Institute of Chemical Physics, Chinese Academy of Sciences, Dalian 116023, Liaoning, China

Abstract: Meso-microporous composites show great promise for catalysis because of their variously-sized porous structures. A series of composites containing uniform mesopores and MFI zeolitic channels were prepared by a template-free sol-gel method. The composite containing silicalite-1 structures was found to be much more hydrothermally stable than MCM-41. The composites with ZSM-5 structures showed higher catalytic activity and resistance to deactivation than commercial HZSM-5 in the catalytic cracking reaction of 1,3,5-triisopropylbenzene. The conversion and catalytic cracking product distribution of 1,3,5-triisopropylbenzene depended highly on the mesopore size of the composites. Higher conversions and small molecule cracking products were obtained using composites with smaller mesopores.

Key words: meso-microporous composite; MFI zeolite; hydrothermal stability; 1,3,5-triisopropylbenzene; catalytic cracking

沸石材料具有高比表面积、吸附能力和离子交换能力以及规则排列的孔道或笼(0.3~1.5 nm), 已经广泛应用于吸附和催化等工业过程, 其接近大多数小分子尺寸的精确的孔道结构使得沸石材料在许多催化反应中表现出不同类型的择形选择性[1], 但同时它们较小的孔道尺寸带来了扩散和传质的限制, 对于一些涉及到大分子的催化反应, 沸石材料也常常无能为力. 自从有序介孔材料MCM-41[2,3]被成功合成以来, 介孔材料因其较大的孔径(2~50 nm)对大分子催化有利的特点得到了人们的广泛关注, 但与传统微孔沸石材料相比, 介孔材料无定形的孔壁结构使其水热稳定性较差、酸性较弱[4].

根据“介孔-微孔复合材料有可能结合不同尺度孔结构的优点”这一思路, 研究者们尝试了多种方法来合成介孔-微孔复合材料, 其中比较有效的方法主要有两种: (1) 由Pinnavaia等[5,6]和肖丰收等[7,8]开发的沸石前驱体自组装方法, 得到的介孔材料具有沸石结构的孔壁; (2) 在沸石合成过程中加入不同类型的模板剂, 诸如碳纳米粒子[9]、碳纳米管[10]、碳气凝胶[11,12]等硬模板, 聚合物[13,14]或者表面活性剂[15,16]

收稿日期: 2010-04-30. 接收日期: 2010-11-26.

联系人: 熊国兴. Tel: (0411) 84379182; Fax: (0411) 84694447; E-mail: gxxiong@dicp.ac.cn
杨维慎. Tel: (0411) 84379073; Fax: (0411) 84694447; E-mail: yangws@dicp.ac.cn

基金来源: 中国石油化工股份有限公司科学技术研究开发项目(X503008); 国家自然科学基金(20321303).
本文的英文电子版由 Elsevier 出版社在 ScienceDirect 上出版(http://www.sciencedirect.com/science/journal/18722067).

等软模板, 得到的沸石晶体包含一定数量的介孔. 至于介孔-微孔复合材料的无模板剂合成法, 高温水蒸气脱铝、酸处理脱铝[17]和碱处理脱硅[18]的方法常常产生具有较宽孔径分布的介孔. 我们曾开发了一种无模板剂的溶胶凝胶法, 从沸石前驱体溶胶出发, 制备的一系列介孔-微孔复合材料具有交联的蠕虫状介孔或无规排列的晶间介孔, 其孔径在2~30 nm范围内可调[19~21]. 本文考察了这些介孔-微孔复合材料的水热稳定性及其在1,3,5-三异丙苯裂化反应中的催化性能.

1 实验部分

1.1 介孔-微孔复合材料的制备

1.1.1 MFI 沸石前驱体溶胶的制备

将20.4 g 20%的四丙基氢氧化铵(TPAOH, Fluka公司)水溶液滴入16.7 g正硅酸乙酯(TEOS, 98%, 北京市益利精细化学品有限公司)中, 形成的油状液搅拌5 min后, 再加入19.8 g二次蒸馏水, 最终混合液的摩尔比为1.0TEOS:0.25TPAOH:25H_2O, 室温继续搅拌30 min后, 在50 ºC继续反应48 h, 自然冷却到室温得到清晰的silicalite-1沸石前驱体溶胶.

在搅拌中, 将25.4 g 20%的TPAOH水溶液加入到20.8 g TEOS和0.4 g异丙醇铝(Al(*i*-OPr)$_3$, 99.5%, 天津市津科精细化工研究所)的混合悬浊液中, 得到摩尔比为 1.0TEOS:0.02Al(i-OPr)$_3$:0.25TPAOH:11.3H_2O的混合液, 在50 ºC继续搅拌48 h, 自然冷却到室温得到清晰的ZSM-5沸石前驱体溶胶.

1.1.2 MFI 沸石前驱体干凝胶的制备

将前述制得的MFI沸石前驱体溶胶倾入清洁的培养皿中, 称重后转入真空干燥箱(30 ºC, 6.67 kPa)中干燥, 最终得到恒重的透明片状干凝胶材料, silicalite-1和ZSM-5沸石前驱体干凝胶中的氧化硅含量分别为7.0×10^{-3} mol/g和7.7×10^{-3} mol/g, 干凝胶材料研磨后过100目筛待用.

1.1.3 干凝胶的溶剂(水)热处理

将具有不同羟基密度的溶剂丙三醇(≥99.0%, 鞍山智奥化学试剂研究所)、乙二醇(99.8%, 天津市博迪化工有限公司)或二次蒸馏水用作MFI沸石前驱体干凝胶溶剂(水)热晶化的介质, 干凝胶粉末与溶剂(SiO_2:溶剂=1:150, 摩尔比)混合后装入不锈钢反应釜的聚四氟乙烯内衬中, 密闭后在不同温度的烘箱中反应24 h, 自然冷却至室温后, 产物过滤, 用二次蒸馏水洗涤至滤液pH值接近中性, 然后转入30 ºC真空干燥箱中干燥, 550 ºC (升温速率1 ºC/min)焙烧6 h除去残留的有机试剂, 得到最终介孔-微孔复合材料, 样品记为S-X-*y*或Z-X-*y*, 其中S和Z分别代表干凝胶类型为silicalite-1和ZSM-5; X代表晶化介质, 对于丙三醇、乙二醇和水, 分别用G, A和W表示; *y*代表热处理的温度. 这里我们将报道5种纯硅和硅铝介孔-微孔复合材料: S-G-130, Z-G-130, Z-A-130, Z-A-180和Z-W-100.

1.2 介孔 MCM-41 的制备

在40 ºC, 将0.3 g氢氧化钠(≥96.0%, 天津市科密欧化学试剂有限公司)和1.7 g十六烷基三甲基溴化铵(CTAB, ≥99.0%, 国药集团化学试剂有限公司)溶于144 ml二次蒸馏水, 得到的溶液冷却至室温后再滴加8.3 g TEOS, 继续搅拌15 min, 得到的悬浊液装入不锈钢反应釜的聚四氟乙烯内衬中, 密闭后在120 ºC的烘箱中反应3 d, 产物洗涤、干燥后, 在550 ºC焙烧6 h除去模板剂CTAB. 另一对比样品HZSM-5为南开大学催化剂厂生产的商品沸石, 其硅铝比为25.

1.3 样品的表征

溶胶样品的粒度分布由N4 Plus型(Coulter公司)粒度仪测得, 测试条件: 10 mW He-Ne激光器, 入射光与检测器夹角为90°, 运行时间120 s. 材料的X射线衍射(XRD)表征在Rigaku D/max-2500PC型X射线衍射仪上进行, Cu K_α线, 低角区域(2θ=1°~10°)管电压40 kV, 电流30 mA, 广角区域(2θ=5°~50°)管电压40 kV, 电流100 mA, 扫描步长0.02°. 样品混合50倍重量的KBr压片后利用Nicolet Impact 410型傅里叶变换红外光谱仪测其红外谱图(FT-IR), 谱图分辨率4 cm^{-1}, 扫描次数32次, 扫描范围400~4000 cm^{-1}, 谱图分析和仪器控制通过Nicolet OMNIC软件完成. 样品的N_2吸附-脱附等温线在OMNISOR-100CX型全自动物理/化学吸附仪上测定, 样品在350 ºC和1.33×10^{-4} Pa真空度下预处理3 h除去物理吸附的水分, 利用HK方法由吸附支计算样品的微孔孔径分布, 利用BJH方法由脱附支计算样品的介孔孔径分布.

1.4 样品的水热稳定性和催化裂化性能测试

将0.1 g样品与20 g二次蒸馏水混合均匀后, 密

闭在不锈钢反应釜的聚四氟乙烯内衬中, 于 180 °C 处理 12 h 以考察样品的水热稳定性. 样品的催化裂化性能测试则以 1,3,5-三异丙苯为探针分子, 在 HP 4890D 型气相色谱仪改装的微型脉冲反应器上进行. 反应温度 400 °C, 催化剂用量 50 mg (40~60 目), 在流动氮气气氛下 400 °C 预处理 1 h; 1,3,5-三异丙苯进样量 0.1 μl, N_2 为载气, 流速 20 ml/min; 裂化产物在线分离和检测, 使用 HP-5 型毛细管柱 (长度 15 m, 内径 0.530 mm, 液膜厚度 1.50 μm, 程序升温由 40 至 200 °C 分离裂化产物) 和 FID 检测器 (检测器温度 250 °C).

2 结果与讨论

2.1 MFI 沸石前驱体溶胶的粒度分布

激光散射粒度分析仪的测试结果表明, 两种沸石前驱体溶胶都具有非常均一的粒度分布, 其中 silicalite-1 前驱体溶胶约 97% 的溶胶粒子分布在 6~12 nm, 平均粒径为 8.8 nm; 而 ZSM-5 前驱体溶胶除了由于 TEOS 和 Al(*i*-OPr)$_3$ 在碱性溶液中快速水解和缩聚产生的极少数大胶粒 (约 100 nm) 外, 85% 的胶粒尺寸为 11.9 nm. de Moor 等[22,23]用小角 X 射线散射技术观察到在 MFI 沸石的合成体系中包括两种前驱体粒子 (2.8 nm 的初级结构单元和大约 10 nm 的初级结构单元聚集体), 因此可认为本文制备的 MFI 沸石前驱体溶胶粒子也是由沸石初级结构单元聚集而成的.

2.2 XRD 和 FT-IR 结果

图 1 为不同样品的 XRD 谱. 可以看出, 焙烧前后的 MCM-41 在 1°~6°范围内出现几个特征衍射峰, 与文献报道结果相似[3], 表明样品中存在有序的介孔结构, 而所有介孔-微孔复合材料在 1°~10°没有任何衍射峰出现, 表明它们不具有有序排列的介孔孔道. 除了 Z-W-100 样品外, 其它的介孔-微孔复合材料仅在 15°~30° 出现一个很宽的衍射峰 (与图 1 中 Z-G-130 样品相似), 表明它们的沸石晶化有序度是小于 4~5 个沸石单胞 (晶粒尺度则小于 8~10 nm)[24]. 尽管它们的有序度不足以利用 XRD 技术检测到, 但是它们的 FT-IR 谱 (见图 2) 在 550~560 cm^{-1} 出现了对应于 MFI 沸石结构单元中双环振动的吸收峰, 证实了其中 MFI 沸石结构的存在[25]. 干凝胶在 100 °C 水热处理制备的 Z-W-100 样品则出现了一系列 ZSM-5 沸石的特征衍射峰, 由 Scherrer 公式计算得到其垂直

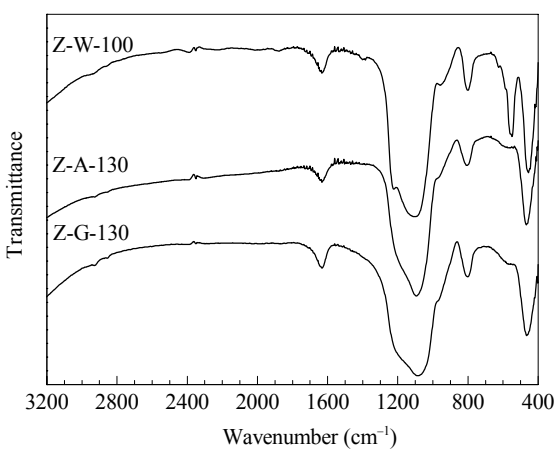

图 2 Z-G-130, Z-A-130 和 Z-W-100 样品的 FT-IR 谱

Fig. 2. FT-IR spectra of the studied samples. Z-A-130: the sample prepared by crystallizing ZSM xerogel and glycol at 130 °C.

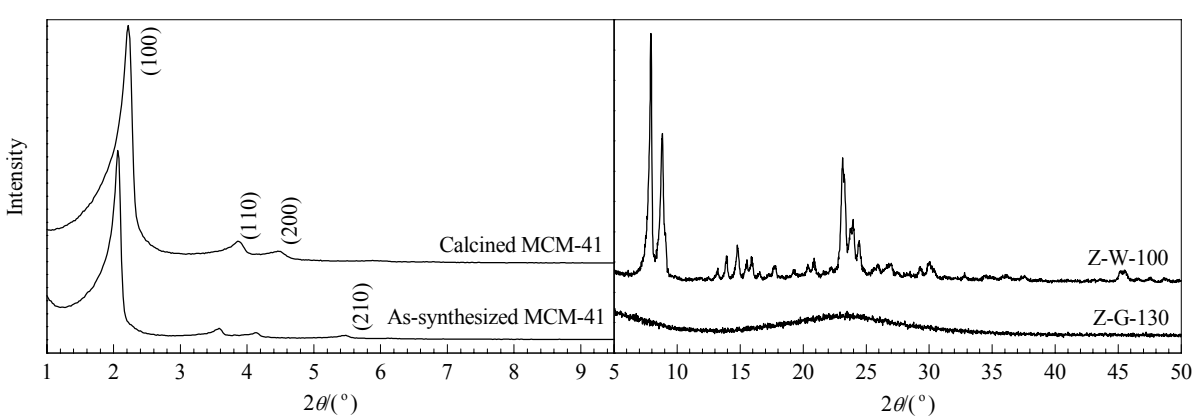

图 1 MCM-41, Z-G-130 和 Z-W-100 样品的 XRD 谱

Fig. 1. XRD patterns of the studied samples. Z-G-130: the sample prepared by crystallizing ZSM-5 xerogel and glycerol at 130 °C; Z-W-100: the sample prepared by crystallizing ZSM-5 xerogel and water at 100 °C.

于(011)晶面方向上的晶粒尺寸约为50.4 nm.

2.3 N_2吸附-脱附等温线结果

图3为各样品的N_2吸附-脱附等温线. 可以看出,除了Z-W-100样品外,其它介孔-微孔复合材料的等温线都可以归属为I和IV复合型,随着晶化介质分子中羟基数量的减少(从丙三醇、乙二醇到水),滞后环出现的位置向高相对压力范围移动,表明样品的介孔孔径逐渐增大,其形状也由H2型开始向H1型转变,表明其介孔结构由墨水瓶形孔逐步转为狭缝形孔[26],较高的热处理温度也倾向于获得更大的介孔孔径.

根据我们前期的实验结果[19],其介孔的形成机理如下. 在真空干燥过程中,MFI沸石初级结构单元和它们的聚集体(溶胶胶粒)通过紧密堆积形成干凝胶,既然溶胶胶粒的粒度是均一的,那么干凝胶中的孔也应该是均一的. 在溶剂热处理过程中,溶胶胶粒和沸石初级结构单元将分别作为沸石形成的晶核和氧化铝氧化硅物种的来源. 因此,晶化介质中氢键作用力的强弱,将直接影响到活性物种的扩散,进而影响到沸石的生长过程,最终在干凝胶中形成不同尺度的沸石纳米晶. 由于在干凝胶体系中存在过饱和的氧化铝和氧化硅物种,这些纳米晶将连生形成最终材料的孔壁结构,介孔则作为晶体间隙孔而存在. 相比较丙三醇和乙二醇而言,水为氧化铝和氧化硅物种提供了较高的溶解度和扩散速率,导致了更快的沸石生长速率,使得样品中介孔孔径均一性受到一定的影响. 前期研究表明[21],将水热处理温度降至80 ºC能够获得均一分布的介孔(孔径为4.5 nm),同时随着水热温度的上升,组成多孔结构的球形纳米粒子由小于10 nm (80 ºC)增长到30 nm (100 ºC)和200 nm (130 ºC).

S-G-130样品在180 ºC水热处理12 h后所得的S-G-130(HT)样品介孔孔径虽略有增加(从3.1到3.8 nm,见图4和表1),但仍维持其均一度和大部分的孔体积,比表面积则下降为原始样品的51.4%. 而介孔MCM-41在水热处理12 h后,其比表面积由原始样品的847.8 m^2/g大幅度降至12.2 m^2/g,其介孔结构完全消失. 由此可见,介孔-微孔复合材料S-G-130较传统的介孔材料MCM-41具有显著改善的水热稳定性. 从S-G-130(HT)样品迅速扩大的微孔孔径来看,其比表面积的下降主要是由于一部分微孔的融合,我们推测在水热处理过程中, Si-O-Si结构的水解过程由于沸石结构的存在而被部分抑制,同时沸石结构的介孔孔壁也具有更高的机械强度(我们应该注意到,水热稳定性考察是在180 ºC下进行,此时体系中压强可达1 MPa),使得介孔-微孔复合材料具有更高的水热稳定性.

2.4 不同样品的催化裂化性能

以1,3,5-三异丙苯为催化裂化原料,考察了不同样品的裂化活性和选择性. 在反应条件下,以高温脱活的石英砂作为空白对比样时,未检测到任何裂化产物生成,因此可以忽略1,3,5-三异丙苯的热裂化反

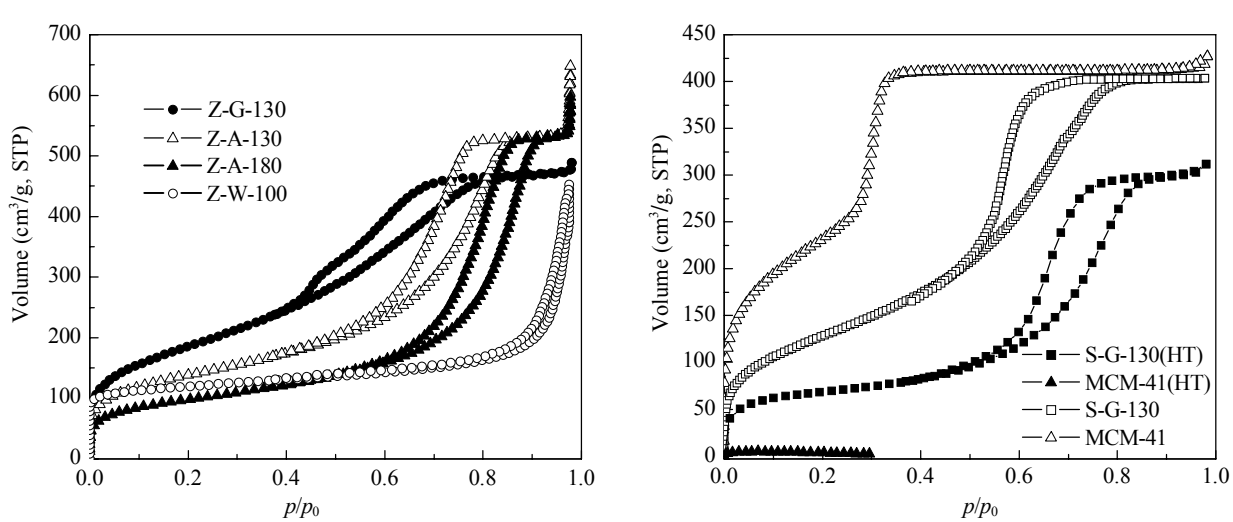

图3 不同样品的N_2吸附-脱附等温线

Fig. 3. N_2 adsorption/desorption isotherms of the studied samples. HT represents hydrothermal-treated samples at 180 ºC.

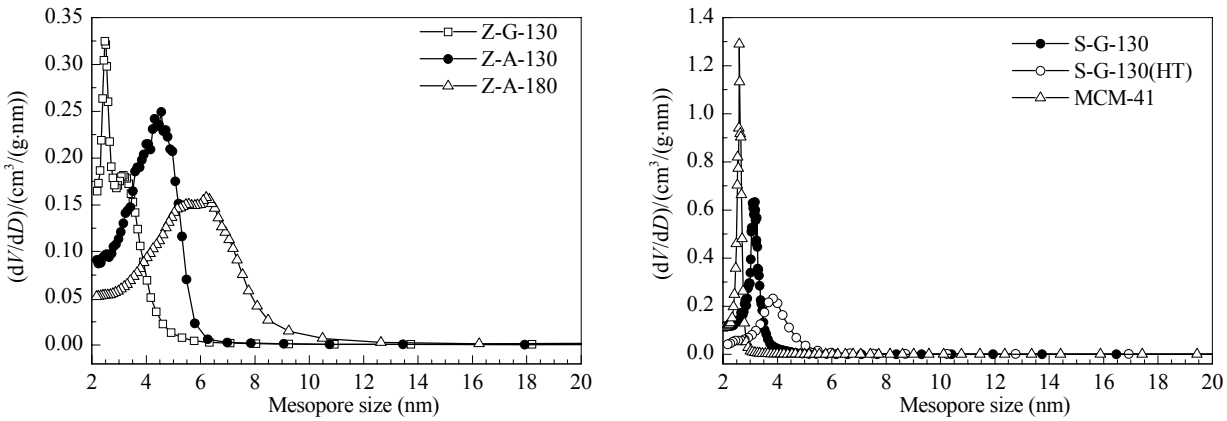

图 4 不同样品的介孔孔径分布

Fig. 4. Mesopore size distributions of the studied samples.

表 1 不同样品的比表面积和孔结构数据

Table 1 Specific surface areas and pore structural data of the studied samples

Sample	A_{BET} (m^2/g)	V_{meso} (cm^3/g)	V_{micro} (cm^3/g)	D_{meso} (nm)	D_{micro} (nm)
S-G-130	473.1	0.48	0.14	3.1	0.57
S-G-130(HT)	243.3	0.35	0.11	3.8	1.01
MCM-41	847.8	0.27	0.36	2.6	wide
Z-G-130	675.5	0.66	0.06	2.5	0.53
Z-A-130	499.3	0.77	0.04	4.3	0.56
Z-A-180	354.6	0.77	0.03	6.2	0.57
Z-W-100	464.9	0.48	0.11	wide	0.54

应对材料催化裂化性能的影响. 图 5 为不同脉冲进样次数后不同样品上 1,3,5-三异丙苯的转化率. 可以看出, 随着脉冲次数的增加, 介孔-微孔复合材料的催化活性变化不大, 而商品 HZSM-5 沸石的催化活性则快速降低. 这是由于 1,3,5-三异丙苯的动力学直径约为 0.74 nm, 大于 ZSM-5 沸石的微孔开口尺寸, 所以商品 HZSM-5 的催化裂化活性位主要由外表面的酸性位所提供, 这些酸性位因积炭而快速失活, 而介孔-微孔复合材料催化裂化活性则由介孔内的酸性位所提供, 在一定程度上限制了积炭的形成.

表 2 为脉冲进样 21 次后 1,3,5-三异丙苯在不同样品上催化裂化产物的分布和转化率. Z-G-130 样品上的反应转化率高达 94.2%, 且异丙苯的选择性达到 42.9%, 而在 Z-A-130 上的转化率和异丙苯选择性只有 41.2% 和 8.9%. 一方面是由于 Z-G-130 样品的介孔孔径 (2.5 nm) 与 1,3,5-三异丙苯的动力学直径比较接近, 介孔内部存在的附加势场预活化了反应物分子, 使其具有较高的催化裂化活性, 而 Z-A-130 样品的介孔孔径 (4.3 nm) 与 1,3,5-三异丙苯的动力学直径相差较大, 不能对反应物分子进行有效的预活化. 另一方面在较大的介孔中裂化产物具有更快的扩散过程, 还未进行下一步的裂化反应即扩散出孔道而进入气相, 导致了在较大介孔的样品上小分子裂化产物选择性较低. Z-A-130 样品和 Z-A-180 样品催化性能的差异则反映了介孔-微孔复合材料中沸石晶化有序度的影响, 两者都具有较大的介孔孔径 (分别为 4.3 和 6.2 nm), 对反应物分子预活化的差别可以忽略, 它们的催化活性将主要取决于样品中酸性位的多少. 在更高温度下晶化的 Z-A-180 样品具有更高的沸石晶化有序度, 相应地也含有更多数量的酸性位. 值得注意的是, 商品 HZSM-5 沸石的催化活性较

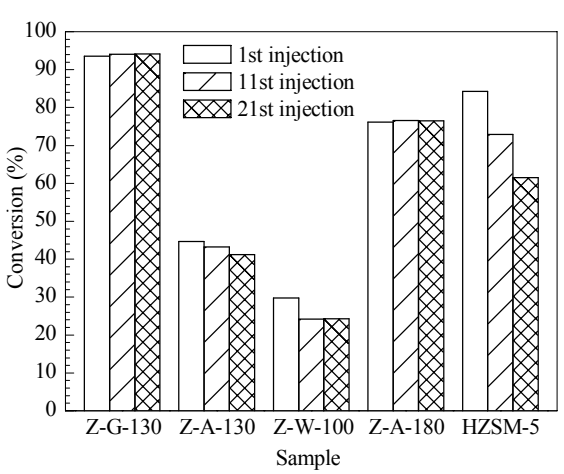

图 5 不同进样次数后 1,3,5-三异丙苯在不同样品上的催化裂化转化率

Fig. 5. Catalytic cracking conversion of 1,3,5-triisopropylbenzene over different samples after different number of injections. Reaction conditions: 400 ºC, 50 mg catalyst, 0.1 μl reactant.

表 2 1,3,5-三异丙苯在不同样品上催化裂化产物的分布和转化率

Table 2 Catalytic cracking product distributions and conversions of 1,3,5-triisopropylbenzene over different samples[a]

Sample	Conversion (%)	Selectivity (%)		
		Benzene	Cumene	DIPB[b]
Z-G-130	94.2	1.8	42.9	55.3
Z-A-130	41.2	0.1	8.9	91.0
Z-A-180	76.5	0.3	18.5	81.2
Z-W-100	24.3	0.4	8.0	91.5
HZSM-5	61.5	65.5	3.7	30.8

[a]Results of the 21st injection; [b]Diisopropylbenzene.

高, 考虑到它与本文制备的介孔-微孔复合材料硅铝比不同 (分别为 25 和 50), 因而各自的酸性位数量不同, 那么 1,3,5-三异丙苯在 Z-G-130、Z-A-130 和 Z-A-180 样品上的裂化转换频率 (TOF) 要普遍高于商品 HZSM-5 沸石. 虽然 Z-W-100 样品的 TOF 与商品 HZSM-5 沸石相差不大, 但由图 5 展示的催化活性变化趋势可以预期, 随着反应的进一步进行, 后者的催化活性因其表面酸性位积炭失活将进一步下降.

3 结论

采用无模板剂的溶胶凝胶法, 从均一粒度的 MFI 沸石前驱体溶胶出发, 经真空干燥和溶剂 (水) 热晶化过程制备了一系列纯硅和硅铝介孔-微孔复合材料. 由于孔壁中沸石结构的存在, 纯硅介孔-微孔复合材料较有序介孔材料 MCM-41 而言, 其水热稳定性显著改善. 在 1,3,5-三异丙苯催化裂化反应中, 硅铝介孔-微孔复合材料表现出比商品 HZSM-5 沸石更高的催化活性和抗积炭失活能力. 基于无模板剂的溶胶凝胶法实验结果, 我们期望建立一个新的沸石结构生长模型, 以预测沸石结构在不同溶剂中及不同温度下的生长情况, 从而指导用于特定反应的介孔-微孔复合催化材料的合成.

致谢 作者感谢张敏博士提供的有益讨论和建设性意见, 感谢盛世善高级工程师和楚文玲副研究员在 N_2 吸附-脱附等温线表征方面提供的帮助.

参 考 文 献

1 Corma A. *Chem Rev*, 1997, **97**: 2373
2 Kresge C T, Leonowicz M E, Roth W J, Vartuli J C, Beck J S. *Nature*, 1992, **359**: 710
3 Beck J S, Vartuli J C, Roth W J, Leonowicz M E, Kresge C T, Schmitt K D, Chu C T W, Olson D H, Sheppard E W, Mccullen S B, Higgins J B, Schlenker J L. *J Am Chem Soc*, 1992, **114**: 10834
4 Tao Y S, Kanoh H, Abrams L, Kaneko K. *Chem Rev*, 2006, **106**: 896
5 Liu Y, Zhang W Z, Pinnavaia T J. *Angew Chem*, *Int Ed*, 2001, **40**: 1255
6 Liu Y, Pinnavaia T J. *J Mater Chem*, 2002, **12**: 3179
7 Zhang Z T, Han Y, Xiao F S, Qiu S L, Zhu L, Wang R W, Yu Y, Zhang Z, Zou B S, Wang Y Q, Sun H P, Zhao D Y, Wei Y. *J Am Chem Soc*, 2001, **123**: 5014
8 韩宇, 肖丰收. 催化学报 (Han Y, Xiao F Sh. *Chin J Catal*), 2003, **24**: 149
9 Jacobsen C J H, Madsen C, Houzvicka J, Schmidt I, Carlsson A. *J Am Chem Soc*, 2000, **122**: 7116
10 Schmidt I, Boisen A, Gustavsson E, Stahl K, Pehrson S, Dahl S, Carlsson A, Jacobsen C J H. *Chem Mater*, 2001, **13**: 4416
11 Tao Y S, Kanoh H, Kaneko K. *J Am Chem Soc*, 2003, **125**: 6044
12 Li W C, Lu A H, Palkovits R, Schmidt W, Spliethoff B, Schuth F. *J Am Chem Soc*, 2005, **127**: 12595
13 Xiao F S, Wang L F, Yin C Y, Lin K F, Di Y, Li J X, Xu R R, Su D S, Schlogl R, Yokoi T, Tatsumi T. *Angew Chem*, *Int Ed*, 2006, **45**: 3090
14 Wang H, Pinnavaia T J. *Angew Chem*, *Int Ed*, 2006, **45**: 7603
15 Choi M, Cho H S, Srivastava R, Venkatesan C, Choi D H, Ryoo R. *Nature Mater*, 2006, **5**: 718
16 Choi M, Na K, Kim J, Sakamoto Y, Terasaki O, Ryoo R. *Nature*, 2009, **461**: 246
17 Janssen A H, Koster A J, de Jong K P. *Angew Chem*, *Int Ed*, 2001, **40**: 1102
18 Groen J C, Moulijn J A, Perez-Ramirez J. *J Mater Chem*, 2006, **16**: 2121
19 Han W, Jia Y X, Yao N, Yang W S, He M Y, Xiong G X. *J Sol-Gel Sci Technol*, 2007, **43**: 205
20 Han W, Jia Y X, Xiong G X, Yang W S. *Stud Surf Sci Catal*, 2007, **165**: 515
21 Han W, Jia Y X, Xiong G X, Yang W S. *Sci Technol Adv Mater*, 2007, **8**: 101
22 de Moor P P E A, Beelen T P M, Komanschek B U, Diat O, van Santen R A. *J Phys Chem B*, 1997, **101**: 11077
23 de Moor P P E A, Beelen T P M, van Santen R A. *J Phys Chem B*, 1999, **103**: 1639
24 On DT, Kaliaguine S. *J Am Chem Soc*, 2003, **125**: 618
25 Jansen J C, van der Gaag F J, van Bekkum H. *Zeolites*, 1984, **4**: 369
26 Sing K S W, Everett D H, Haul R A W, Moscou L, Pierotti R A, Rouquerol J, Siemieniewska T. *Pure Appl Chem*, 1985, **57**: 603

英 译 文

English Text

Zeolites have been applied widely in many industrial processes such as adsorption and catalysis because of their high surface area, adsorption capacity, ion-exchange capacity, and regular arrays of channels and cavities (0.3–1.5 nm). Their intricate channel structures allow the zeolites to have different types of shape selectivity, i.e., for products, reactants, and transition states, which can be used to direct a given catalytic reaction toward the desired product and avoid undesired side reactions [1]. However, the small pore sizes of zeolites result in diffusion and mass transfer limitations especially in the reactions involving large molecules. Since the discovery of MCM-41 in 1992 [2,3], mesoporous materials have attracted much attention because of their potential use as catalysts and catalyst supports for the conversion of large molecules. Compared to conventional zeolites, mesoporous materials have low hydrothermal stability and acidity, which has been attributed to their amorphous pore walls [4].

Since meso-microporous composites can possibly combine the advantages of variously-sized porous structures, researchers have made many attempts to prepare meso-microporous composites. Pinnavaia et al. [5,6] and Xiao et al. [7,8] used surfactant to assemble zeolite precursor for synthesizing mesoporous materials with zeolitic walls. Zeolites with mesopores were also fabricated by the addition of different templates such as rigid templates containing carbon nanoparticles [9], carbon nanotubes [10] and carbon aerogels [11,12] or soft templates containing polymers [13,14] and surfactants [15,16] into the zeolite synthesis solution. As to template-free routes to the meso-microporous composite, steaming, acid-leaching dealumination [17], and alkali-leaching desilication [18] of zeolite crystals often generate mesopores with wide size distributions. In our previous work, we developed a template-free sol-gel method to synthesize a series of meso-microporous composites from a zeolite precursor sol. They were found to consist of interconnected worm-like mesopores or intercrystalline mesopores with irregular arrays and their mesopore sizes could be controlled between 2 and 30 nm [19–21]. In this work, we investigated the hydrothermal stability of several meso-microporous composites and their catalytic performance in the cracking reaction of 1,3,5-triisopropylbenzene.

1 Experimental

1.1 Preparation of the meso-microporous composites

1.1.1 Preparation of the MFI zeolite precursor sol

In a typical silicalite-1 precursor sol synthesis, 20.4 g of the 20% aqueous solution of tetrapropylammonium hydroxide (TPAOH, Fluka) was added to 16.7 g of tetraethyl orthosilicate (TEOS, 98%, Beijing Yili) under vigorous stirring. To the resulting emulsion, 19.8 g of twice distilled water was added. The resulting emulsion with the molar composition of 1.0TEOS:0.25TPAOH:25H_2O was stirred at 50 °C for 48 h to form a clear silicalite-1 precursor sol.

25.4 g of the 20% aqueous solution of TPAOH was added to the mixture of 20.8 g of TEOS and 0.4 g of aluminum isopropoxide (Al(*i*-OPr)$_3$, 99.5%, Tianjin Jinke) under vigorous stirring at room temperature to obtain a turbid solution with the molar composition of 1.0TEOS:0.02Al(*i*-OPr)$_3$:0.25TPAOH:11.3H_2O. Clear ZSM-5 precursor sol was obtained by stirring the turbid solution at 50 °C for 48 h.

1.1.2 Preparation of the MFI zeolite precursor xerogel

Silicalite-1 and the ZSM-5 precursor sol were transferred to clean glass dishes and dried at 30 °C in a vacuum box at 6.67 kPa until they became xerogels. The silica contents in the silicalite-1 and ZSM-5 xerogels were 7.0×10^{-3} mol/g and 7.7×10^{-3} mol/g, respectively.

1.1.3 Solvo/hydrothermal crystallization of the xerogel

Glycerol (≥ 99.0%, Anshan Zhiao), glycol (99.8%, Tianjin Bodi), and twice distilled water were used as media for heat crystallization. A mixture of xerogel and solvent/water (1 SiO_2:150 solvent/water molar ratio) was transferred into Teflon-lined stainless steel autoclaves and solvo/hydrothermal crystallization was carried out at a certain temperature for 24 h. The solid products were filtered, washed, dried at 30 °C in a vacuum box, and calcined in air at 550 °C for 6 h. The calcined samples were designated S-X-*y* or Z-X-*y* (S and Z indicate silicalite-1 and ZSM-5 xerogels, respectively; X represents the crystallization medium such as G = glycerol, A = glycol, and W = water; *y* is the crystallization temperature). For example, S-G-130 was the sample prepared by crystallizing silicalite-1 xerogel and glycerol at 130 °C. We prepared five meso-microporous composites: S-G-130, Z-G-130, Z-A-130, Z-A-180, and Z-W-100.

1.2 Preparation of mesoporous MCM-41

Mesoporous MCM-41 was also synthesized for comparison. 0.3 g of sodium hydroxide (NaOH, ≥ 96.0%, Tianjin Kemiou) and 1.7 g of cetyltrimethylammonium bromide (CTAB, ≥ 99.0%, Shanghai Guoyao) were dissolved in 144 ml of twice distilled water at 40 °C followed by the addition of 8.3 g of TEOS at room temperature. The mixture was stirred for 15 min and transferred into a Teflon-lined stainless steel autoclave to carry out hydrothermal synthesis at 120 °C for 3 d. As-synthesized MCM-41 was filtered, washed, dried, and calcined in air at 550 °C for 6 h.

1.3 Characterization of the samples

The particle size distribution of the precursor sol was measured using a N4 plus laser scattering particle meter (Coulter) equipped with a 10 mW He-Ne laser. X-ray diffraction (XRD) characterization was performed using a Rigaku D/max-2500PC X-ray diffractometer with a copper target at 40 kV and 30 mA (2θ = 1°–10°) or 100 mA (2θ = 5°–50°) with the step size of 0.02°. Fourier transform infrared (FT-IR) spectra were recorded using a Nicolet Impact 410 FTIR spectrometer. A mixture of the sample and KBr was pressed into a thin wafer before the IR measurement. All IR spectra were measured under the following conditions: resolution of 4 cm^{-1}, scan time of 32, and scan range from 400 to 4000 cm^{-1}. N_2 adsorption/desorption isotherms of the samples were measured on a Coulter Omnisorp-100CX apparatus at –196 °C. The solid samples were first degassed at 350 °C under high vacuum (1.33×10^{-4} Pa) for 3 h to remove adsorbed impurities from the pores of the samples before the isotherms were recorded. Mesopore and micropore size distributions were determined using BJH method from desorption branch and HK method from adsorption branch, respectively.

1.4 Hydrothermal stability and catalytic cracking performance

0.1 g of the calcined sample and 20 g of twice distilled water in a Teflon-lined stainless steel autoclave were heated at 180 °C for 12 h to test hydrothermal stability. The catalytic cracking reaction of 1,3,5-triisopropylbenzene over different samples was tested in a home-made pulse microreactor based on a HP 4890D GC system. 50 mg of the catalyst (40–60 mesh) was pretreated under a high purity nitrogen flow at 400 °C for 1 h. 0.1 μl of 1,3,5-triisopropylbenzene was pulse-injected and carried by high pure nitrogen at a flow rate of 20 ml/min into the catalyst layer at 400 °C. The cracking products were separated using a HP-5 capillary column (length: 15 m, inner diameter: 0.530 mm, thickness of liquid film: 1.50 μm) with a programmed-temperature process from 40 to 200 °C and detected by an FID detector at 250 °C.

2 Results and discussion

2.1 Particle size distribution of the MFI zeolite precursor sol

Results from the laser scattering particle meter show that both the MFI zeolite precursor sols have a very uniform particle size distribution. For the silicalite-1 precursor sol, ca. 97% of the sol particles range between 6–12 nm and their mean size is 8.8 nm. For the ZSM-5 precursor sol, most of the sol particles (ca. 85%) have the size of 11.9 nm beside a small amount of larger sol particles with the size of 100 nm generated from the rapid hydrolysis and condensation processes of TEOS and Al(i-OPr)$_3$ in alkaline solution. de Moor et al. [22,23] observed two types of precursor particles (2.8 nm sized primary units and ~10 nm aggregates) in MFI zeolite synthesis systems by small-angle X-ray scattering. Based on these results, sol particles can be thought reasonably to be aggregates of zeolite primary units.

2.2 XRD patterns and FT-IR spectra of the studied samples

XRD patterns of as-synthesized and calcined MCM-41 samples show several typical diffraction peaks between 1° and 6° (Fig. 1). They are similar to the XRD patterns reported in literature [3], which indicates that there are ordered mesoporous structures within these samples. It is different from the ordered mesoporous MCM-41 that no diffraction peaks below 5° appear in the XRD patterns of the meso-microporous composites. These meso-microporous composites do not have mesopores with an ordered array. Their XRD patterns, which are similar to Z-G-130 sample in Fig. 1, only contains wide diffraction peaks located between 15° and 30° except for Z-W-100 sample. The crystalline ordering of the zeolite structures within them is less than 4–5 unit cells or 8–10 nm [24]. Although their ordering is not adequate to be detected by XRD, the appearance of the 550–560 cm^{-1} band that corresponds to the double ring vibration in their FT-IR spectra (Fig. 2) verifies the existence of the MFI zeolite structures [25]. The XRD pattern for Z-W-100 sample that was prepared in water at 100 °C contains a series of typical ZSM-5 zeolite diffraction peaks. Z-W-100 sample has a crystal size of 50.4 nm in the vertical direction of (011) determined using the Scherrer equation.

2.3 Texture properties of the studied samples

The N_2 adsorption/desorption isotherms of meso-microporous composites can be assigned to type I and IV composites except for the Z-W-100 sample (Fig. 3). With a decrease in the number of OH within the crystallization medium molecules (from glycerol, glycol, to water), the hysteresis loop shifts from a low to a relatively high pressure, which indicates the increase in mesopore size from 2.5 nm for Z-G-130 to 4.3 nm for Z-A-130. The shape of the hysteresis loop shows a change from H2 to H1, which indicates the change from ink-bottle-like mesopores to slit-like mesopores [26]. Higher crystallization temperature also benefits the formation of larger mesopores.

Based on our previous experimental results [19], we can speculate on the formation mechanism of the mesopores

within the meso-microporous composites. MFI zeolite primary units and their aggregates in the zeolite precursor sol pack closely in the xerogel during the vacuum drying process. Pores within the xerogel should have a narrow size distribution since the particle size of the precursor sol is uniform. During the solvo/hydrothermal crystallization process, primary units and their aggregates are the source of the alumina-silica species and the nuclei of the zeolite crystals, respectively. Therefore, the intermolecular action of the crystallization medium (mainly hydrogen band) affects directly the diffusion of species, sequentially zeolite growth process. Thus zeolite nanocrystals of different sizes form within the xerogel and intergrow into the walls of the final products because of the existence of a supersaturated alumina-silica species within the xerogel. The mesopores within the meso-microporous composites are interspaces between the zeolite nanocrystals. Compared to glycerol and glycol, water supplies a higher solubility and diffusion rate for the alumina-silica species. The uniformity of the mesopore size in Z-W-100 is destroyed by the rapid zeolite growth process. In our previous work [21], uniformly-sized mesopores (4.5 nm) were obtained by hydrothermal crystallization at 80 °C. SEM images showed that the size of the spherical nanoparticles increased obviously from 10 nm (80 °C) and 30 nm (100 °C) to 200 nm (130 °C).

The hydrothermally-treated S-G-130 sample (S-G-130(HT) sample) retains its mesopores with a narrow size distribution and most pore volume. Its mesopore size increases slightly from the original 3.1 nm to 3.8 nm accompanied by a decrease in BET specific surface area (Fig. 4 and Table 1). Compared to S-G-130(HT), hydrothermal-treated MCM-41 at 180 °C for 12 h disappears its mesoporous structures. Its BET specific surface area decreases obviously from the original 847.8 m^2/g to 12.2 m^2/g. These results show that the meso-microporous composite has remarkably improved hydrothermal stability compared to the conventional mesoporous material. From the large increase in micropore size of the S-G-130(HT) sample we believe that some micropores extend and fuse because of Si-O-Si hydrolysis during hydrothermal treatment. However, the destruction process is suppressed because of the existence of zeolite structures. Moreover, mesopore walls with zeolite structures were found to have higher mechanical strength because hydrothermal stability testing was carried out in an autoclave at 180 °C where 1 MPa exists.

2.4 Catalytic cracking performance of the studied samples

We investigated catalytic cracking activities and selectivities of different samples using 1,3,5-triisopropylbenzene as a reactant. No cracking products were detected over inert quartz sand under the reaction conditions, so a thermal cracking process can be ignored. From Fig. 5 the meso-microporous composites are shown to have similar catalytic activities upon an increase in the injection number whereas the catalytic activity of the commercial HZSM-5 zeolite (Si/Al = 25, Nankai University) decreases rapidly. Since the kinetic diameter of 1,3,5-triisopropylbenzene is ca. 0.74 nm, which is larger than the size of the micropores within the HZSM-5 zeolite, the acidity sites on the external surface of the HZSM-5 zeolite contributes to the catalytic cracking activity. Coke deposition on these acid sites results in a rapid deactivation of the HZSM-5 zeolite. The catalytic cracking activities of the meso-microporous composites results from the acid sites on the mesopore walls where coke deposition is hindered by the limited mesopore size.

Table 2 shows the catalytic cracking product distributions and conversions of 1,3,5-triisopropylbenzene over different samples after 20 injections. The conversion of 1,3,5-triisopropylbenzene and the selectivity for cumene over Z-G-130 sample with a mesopore size of 2.5 nm reaches 94.2% and 42.9%, respectively. For Z-A-130 sample with the mesopore size of 4.3 nm, these values are only 41.2% and 8.9%, respectively. On one hand, the smaller mesopore size of Z-G-130 sample is closer to the kinetic diameter of 1,3,5-triisopropylbenzene, which benefits the pre-activation of the reactant molecules. On the other hand, the cracking products diffuse more rapidly within larger mesopores resulting in a low selectivity for cracking products with small molecular weights.

The difference in the catalytic performance between Z-A-130 sample and Z-A-180 sample mainly results from the number of acid sites within the catalysts since the pre-activation of reactant molecules is not obvious within the larger mesopores. Z-A-180 sample that was prepared at a higher crystallization temperature has a higher zeolite crystalline ordering (i.e. more acid sites). Therefore, higher conversion is obtained over Z-A-180 sample. It should be noted that the commercial HZSM-5 zeolite has a higher catalytic activity. Considering the difference in Si/Al ratio between the meso-microporous composites (Si/Al = 50) and the commercial HZSM-5 (Si/Al = 25), the TOFs of 1,3,5-triisopropylbenzene over the meso-microporous composites are higher than that over the commercial HZSM-5. We can reasonably presume from the change in catalytic activity (Fig. 5) that a further deactivation will occur over commercial HZSM-5 because of coke deposition onto the surface acid sites.

3 Conclusions

A series of silica and aluminosilicate meso-microporous composites were prepared by solvo/hydrothermal crystalli-

zation of the xerogel that was converted from a uniformly-sized MFI zeolite precursor sol. Compared to mesoporous MCM-41, the silica meso-microporous composite shows remarkably improved hydrothermal stability because of the existence of zeolite structures. We also found that aluminosilicate meso-microporous composites show higher catalytic activity and ability against deactivation compared to commercial HZSM-5 zeolite in the catalytic cracking reaction of 1,3,5-triisopropylbenzene. Based on the characterization results of the meso-microporous composites prepared under different conditions such as crystallization solvent and temperature, work is being done to establish a new model of zeolite structure growth for directing synthesis of hierarchical porous catalysts applied in a certain reaction.

Acknowledgments

The authors gratefully acknowledge Dr. Min ZHANG for fruitful discussions, Senior Engineer Shishan SHENG and Associate Prof. Wenling CHU for the measurement of N_2 adsorption/desorption isotherms.

Full-text paper available online at ScienceDirect
http://www.sciencedirect.com/science/journal/18722067